Numerical analysis of the influence of circuit arrangement on a fin-and-tube condenser performance

Cesare Maria Joppolo, Luca Molinaroli *, Alberto Pasini

Dipartimento di Energia, Politecnico di Milano, Via Lambruschini 4, 20156 Milano, Italy

ARTICLE INFO

ABSTRACT

In the present paper a model for the steady-state simulation of fin-and-tube condenser is developed. The model is based on a finite volume approach that divides each tube into small elemental volumes where mass, momentum and energy conservation equations are solved using the effectiveness-NTU method and with appropriate correlations for void fraction, friction factor and heat transfer coefficient calculation. The model is validated against experimental data on two small condensers finding that the calculated heat transfer rate and refrigerant-side pressure drop agree within ±5% and ±21% respectively to the experimental values. The model is then used to numerically analyse the impact of different circuit arrangements on the condenser heat transfer rate, refrigerant-side pressure drop and refrigerant charge.

© 2015 Published by Elsevier Ltd.

1. Introduction

Fin-and-tube heat exchangers are widely used in air-conditioning and refrigeration system both as evaporators and/or condensers. The design of such heat exchangers is generally aimed at finding the best compromise among heat transfer rate, pumping power and manufacturing cost. Optimisation of heat exchanger design is a complex process since the number of parameters that may be varied is very high (e.g. tube diameter, length and internal shape, number of tubes and rows, and fin pitch and shape) and the general finding that the increase of heat transfer area is always beneficial since it leads to an increase of heat exchanger performance may not be true if the pressure drop and related pumping power or the total manufacturing costs are considered. Moreover, if installation or space constraints are introduced, the heat exchanger dimensions may be hardly varied and component optimisation requires that circuit arrangement has to be considered.

In the last few decades, many simulation tools have been developed and validated to predict finned condenser performance accounting for circuit arrangement [2,3,8,19,16,22,7,29] and genetic algorithm methods to optimise the refrigerant circuit arrangement are proposed [9,28]. However, when the problem of circuitry optimisation is addressed, generally the maximum heat exchanger capacity [9,28], the minimum heat transfer surface under the same heat transfer rate [28] or the minimum entropy production [29] are sought without providing any information about refrigerant-side pressure drop or refrigerant charge.

Therefore, in this paper a simulation tool for the prediction of fin-and-tube condenser performance is developed and validated and it is then used to analyse the influence of circuit arrangement on condenser heat transfer rate, refrigerant-side pressure drop and refrigerant charge.

---

* Corresponding author. Fax: +39 02 23993913.
E-mail address: luca.molinaroli@polimi.it (L. Molinaroli).

Nomenclature

		θ	angle (rad)
		ξ	void fraction (dimensionless)
A	area (m^2)	ρ	density (kg m^{-3})
c_P	isobaric specific heat (J kg^{-1} K^{-1})	σ	contraction ratio of cross-sectional area (dimensionless)
d	diameter (m)		
f	friction factor (dimensionless)	*ACC*	acceleration
G	mass flux (kg m^{-2} s^{-1})	*AIR*	air
g	gravitational constant (m s^{-2})	*AVE*	average
h	enthalpy (J kg^{-1}) or heat transfer coefficient (W m^{-2} K^{-1})	*CONT*	contact
		ELE	elemental volume
k	thermal conductivity (W m^{-1} K^{-1})	*EXT*	external
l	length (m)	*FIN*	fin
$\dot{m}$	mass flow rate (kg s^{-1})	*FOU*	fouling
M	mass (kg)	*FRIC*	friction
NTU	number of transfer units (dimensionless)	*GRAV*	gravitation
p	pressure (Pa) or pitch (m)	*IN*	inlet
$\dot{Q}$	heat transfer rate (W)	*INT*	internal
R	thermal resistance (m^2 K W^{-1})	*LIQ*	liquid
T	temperature (K)	*MIN*	minimum
t	thickness (m)	*OUT*	outlet
U	overall heat transfer coefficient (W m^{-2} K^{-1})	*REF*	refrigerant
v	velocity (m s^{-1})	*TOT*	total
x	quality (dimensionless)	*TUB*	tube
ε	effectiveness (dimensionless)	*VAP*	vapour
η	efficiency (dimensionless)	*W*	wall

2. Model description

The model of the fin-and-tube condenser is developed using a finite volume approach. The generic heat exchanger (Fig. 1(a)) is divided into small, tube-centered elemental volumes (Fig. 1(b)) and a unique referential code is assigned to each of them. The referential code is composed by three numbers where the first one identifies the tube under analysis in a given row, the second one refers to the row under consideration and the third one identifies the elemental volume as shown in Fig. 1(b). The shape of the elemental volumes changes according to tubes' arrangement, being a rectangular cuboid for in-line arrangement and a hexagonal prism for staggered one as shown in Fig. 2.

The mass, momentum and energy equations are applied to each elemental volume and solved introducing the following assumptions:
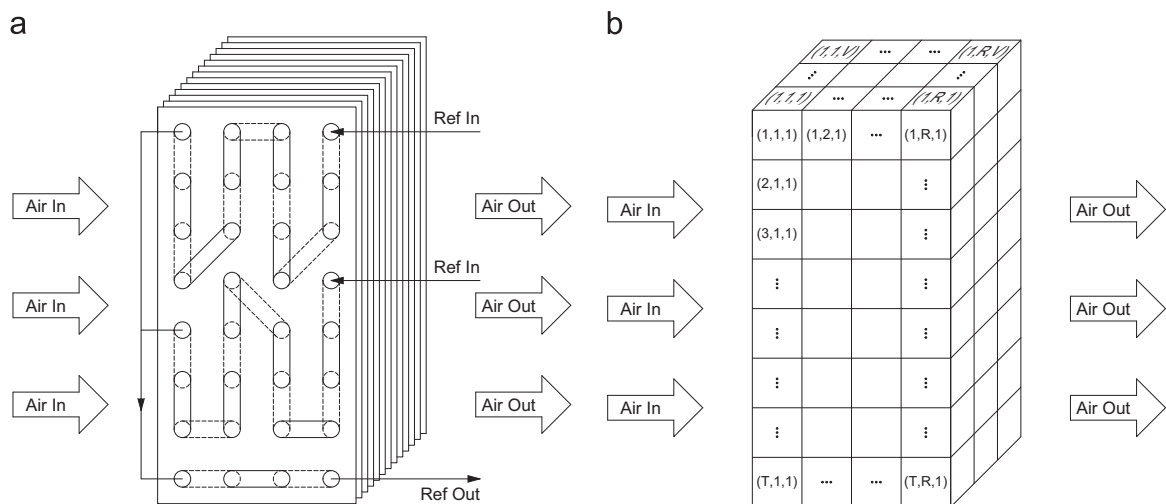

Fig. 1. Fin-and-tube condenser (a) and volume discretization (b) (T = number of tubes per row, R = number of rows and V = number of sub-volumes per tube.)
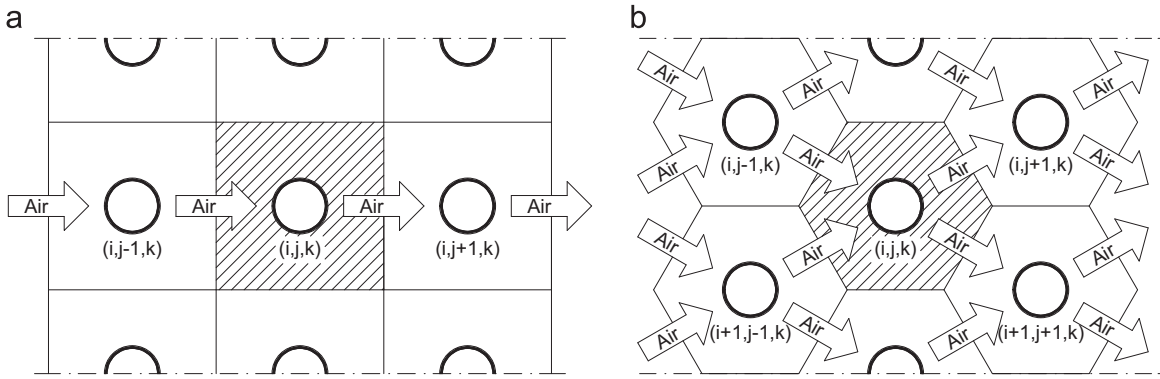
a

b

Fig. 2. Shape of elemental volume for in-line (a) and staggered (b) tube arrangements.

1. The fin-and-tube condenser operates in a steady-state regime.
2. Phase change occurs when bulk enthalpy reaches saturated enthalpy at given pressure (i.e., no superheated condensation).
3. Kinetic and potential energy are negligible.
4. Axial heat conduction through tube thickness is negligible.
5. Radiation heat transfer with the surrounding is negligible.
6. Return bends, joints, splits and headers are adiabatic.
7. Refrigerant and air properties are constant at the elemental volume level.

Refrigerant-side and air-side mass, momentum and energy equations applied to each elemental volume are detailed in next sections.

2.1. Refrigerant-side equations

The refrigerant-side mass, momentum and energy equations applied to each elemental volume are the following (see Fig. 3 for symbols):

$$\dot{m}_{REF,(i,j,k)} = \dot{m}_{REF,(i,j,k+1)} \tag{1}$$

$$p_{REF,(i,j,k)} = p_{REF,(i,j,k+1)} + \Delta p_{REF,FRIC,(i,j,k)} + \Delta p_{REF,GRAV,(i,j,k)} + \Delta p_{REF,ACC,(i,j,k)} \tag{2}$$

$$\dot{m}_{REF,(i,j,k)} h_{REF,(i,j,k)} = \dot{Q}_{(i,j,k)} + \dot{m}_{REF,(i,j,k+1)} h_{REF,(i,j,k+1)} \tag{3}$$

(Eqs. (1)–3) are general and apply either during single-phase flow (desuperheating or subcooling of the refrigerant) or during two-phase flow (refrigerant condensation) with the noteworthy difference that during two-phase flow, momentum (Eq. (2)) and energy (Eq. (3)) equations have to be solved together since the refrigerant pressure drop induces a saturation temperature drop which, in turn, influences heat transfer rate (see Section 2.3).

The friction, gravitation and acceleration contribution to refrigerant-side pressure drop are calculated as follows:
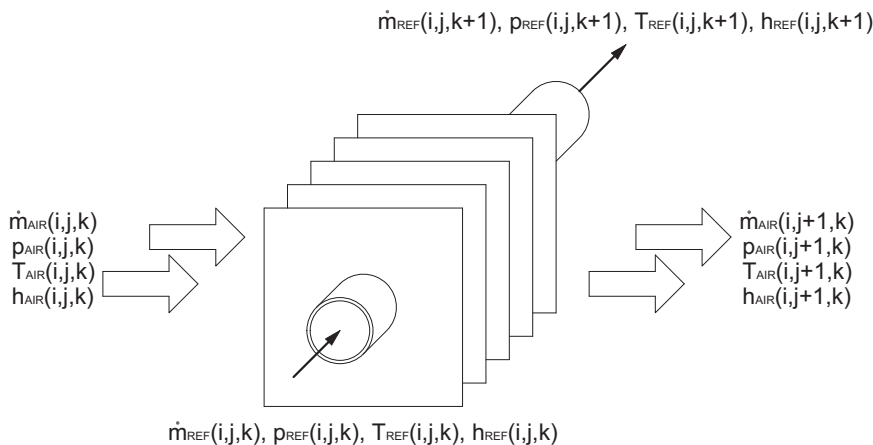
$\dot{m}_{REF}(i,j,k+1), p_{REF}(i,j,k+1), T_{REF}(i,j,k+1), h_{REF}(i,j,k+1)$

$\dot{m}_{AIR}(i,j,k)$
$p_{AIR}(i,j,k)$
$T_{AIR}(i,j,k)$
$h_{AIR}(i,j,k)$

$\dot{m}_{AIR}(i,j+1,k)$
$p_{AIR}(i,j+1,k)$
$T_{AIR}(i,j+1,k)$
$h_{AIR}(i,j+1,k)$

$\dot{m}_{REF}(i,j,k), p_{REF}(i,j,k), T_{REF}(i,j,k), h_{REF}(i,j,k)$

Fig. 3. Generic tube elemental volume with refrigerant and air parameters.

$$\Delta p_{REF,FRIC,(i,j,k)} = f \frac{l_{ELE,(i,j,k)}}{d_{INT,TUB}} \frac{G^2_{REF,(i,j,k)}}{2\rho_{REF,AVE,(i,j,k)}}$$
(4)

$$\Delta p_{REF,GRAV,(i,j,k)} = \rho_{REF,AVE,(i,j,k)} l_{ELE,(i,j,k)} g \, \sin(\theta)$$
(5)

$$\Delta p_{REF,ACC,(i,j,k)} = G^2_{REF,(i,j,k)} \left\{ \frac{[1 - x_{(i,j,k+1)}]^2}{\rho_{LIQ} \xi_{(i,j,k+1)}} + \frac{x^2_{(i,j,k+1)}}{\rho_{VAP} \xi_{(i,j,k+1)}} - \frac{[1 - x_{(i,j,k)}]^2}{\rho_{LIQ} \xi_{(i,j,k)}} - \frac{x^2_{(i,j,k)}}{\rho_{VAP} \xi_{(i,j,k)}} \right\}$$
(6)

During single-phase flow, acceleration term is neglected and Blasius's correlation [21] is used to estimate friction factor for smooth tubes whereas Afroz and Miyara [1] correlation is used for microfin ones. On the other hand, during two-phase flow the most recent flow pattern based model for smooth tube proposed by Quibén and Thome [20] or the formulation proposed by Cavallini et al. [4] for microfin tube are used.

Finally, for each element the refrigerant charge is computed according to the following equation:

$$M_{REF,(i,j,k)} = [\xi_{(i,j,k)}\rho_{VAP} + \left(1 - \xi_{(i,j,k)}\right)\rho_{LIQ}]\pi\frac{d^2_{INT,TUB}}{4}l_{ELE,(i,j,k)}$$
(7)

where the liquid and vapour density are taken at the average saturation conditions during two-phase flow and at the average inlet–outlet element conditions during single-phase one. Void fraction is estimated using the logarithmic mean void fraction model proposed by El Hajal et al. [10].

2.2. Air-side equations

For air-side, a distinction between in-line tube arrangement and staggered tube arrangement has to be introduced in developing mass and energy equations. Indeed, the shape of the elemental volumes changes according to tubes arrangement as shown in Fig. 2 and, consequently, the mass flow rate and the enthalpy of air entering in any elemental volume can be either the same as those that flow out of the preceding one, as in the in-line arrangement, or the result of a mixing process between the two flows that flow out of the preceding elemental volumes, as in the staggered arrangement.

Therefore, for in-line arrangement mass and energy equations are

$$\dot{m}_{AIR,(i,j,k)} = \dot{m}_{AIR,(i,j+1,k)}$$
(8)

$$\dot{m}_{AIR,(i,j,k)} h_{AIR,(i,j,k)} + \dot{Q}_{(i,j,k)} = \dot{m}_{AIR,(i,j+1,k)} h_{AIR,(i,j+1,k)}$$
(9)

Whereas for staggered arrangement the mass and energy equations become

$$\frac{1}{2}(\dot{m}_{AIR,(i,j,k)} + \dot{m}_{AIR,(i-1,j,k)}) = \dot{m}_{AIR,(i,j+1,k)}$$
(10)

$$\frac{1}{2}(\dot{m}_{AIR,(i,j,k)} h_{AIR,(i,j,k)} + \dot{m}_{AIR,(i-1,j,k)} h_{AIR,(i-1,j,k)}) + \dot{Q}_{(i,j,k)} = \dot{m}_{AIR,(i,j+1,k)} h_{AIR,(i,j+1,k)}$$
(11)

Concerning momentum equation, in the air-side the influence of pressure variation on heat transfer rate is negligible since the fluid does not undergo a phase change. Consequently, the momentum equation is solved separately from the energy equation and only the whole pressure drop at condenser scale, rather than the one at elemental volume scale, is calculated

$$p_{AIR,IN} = p_{AIR,OUT} + \Delta p_{AIR,FRIC}$$
(12)

The frictional term in Eq. (12) is calculated according to the following formulation [17] and using appropriate correlation [25,27,24] to estimate the friction factor parameter depending on fin shape and tube arrangement:

$$\Delta p_{AIR,FRIC} = \frac{G^2}{2\rho_{IN}}\left[f\frac{A_{TOT}}{A_{MIN}}\frac{\rho_{IN}}{\rho_{AVE}} + (1 + \sigma^2)\left(\frac{\rho_{IN}}{\rho_{OUT}} - 1\right)\right]$$
(13)

2.3. Elemental volume heat transfer

In the present model, each elemental volume considers both the tube and the fins associated to its length, as shown in Fig. 3, and is analysed as an independent cross-flow heat exchanger where the air is the unmixed stream and the refrigerant is the mixed one. The heat transfer rate between refrigerant and air is calculated using the $\varepsilon - NTU$ method:

$$\dot{Q}_{(i,j,k)} = \varepsilon_{(i,j,k)}(\dot{m}c_P)_{MIN,(i,j,k)}(T_{REF,(i,j,k)} - T_{AIR,(i,j,k)})$$
(14)

where the effectiveness is calculated using specific formulation for single-phase and two-phase flow [11] and $NTU_{(i,j,k)}$ is calculated according to the following equations:

$$NTU_{(i,j,k)} = \frac{(UA)_{(i,j,k)}}{(\dot{m}c_P)_{MIN,(i,j,k)}}$$
(15)

$$\frac{1}{(UA)_{(i,j,k)}} = R_{REF,(i,j,k)} + R_{FOU,INT} + R_{W,(i,j,k)} + R_{FOU,EXT} + R_{AIR,(i,j,k)} \tag{16}$$

In Eq. (16) fouling resistances are user supplied parameter, whereas refrigerant-side, wall and air-side thermal resistances are calculated as follows:

$$R_{REF,(i,j,k)} = \frac{1}{\pi d_{INT} l_{ELE,(i,j,k)} h_{REF,(i,j,k)}} \tag{17}$$

$$R_{W,(i,j,k)} = \frac{\ln(d_{EXT,TUB}/d_{INT,TUB})}{2\pi k_{TUB} l_{ELE,(i,j,k)}} + \frac{\ln[(d_{EXT,TUB} + 2t_{FIN})/d_{EXT,TUB}]}{2\pi k_{FIN} l_{ELE,(i,j,k)}} \tag{18}$$

$$R_{AIR,(i,j,k)} = \frac{1}{h_{AIR,(i,j,k)}} \frac{p_{FIN}}{l_{ELE,(i,j,k)}} \left(\frac{1}{\eta_{FIN} A_{FIN,(i,j,k)}} + \frac{1}{\pi (d_{EXT,TUB} + 2t_{FIN}) l_{ELE,(i,j,k)} (p_{FIN} - t_{FIN})} \right) \tag{19}$$

The refrigerant-side convective heat transfer coefficient is calculated using Gnielinski's correlation [13] in the single-phase flow and using the model proposed by Thome et al. [23] during the condensation regime in smooth tubes whereas the correlation proposed by Copetti et al. [6] or the model proposed by Cavallini et al. [5] are respectively used during single-phase flow or condensation in microfin tubes. The air-side convective heat transfer coefficient is calculated using the appropriate correlation depending on fin shape and tube arrangement [25,27,24]. It is worth noting that the velocity of the air used in the just mentioned correlations is the actual one that depends on air flow rate distribution in the frontal surface. Since each tube is divided into small elemental volumes, it is therefore possible to account for bi-dimensional air mal-distribution in the simulation of the fin-and-tube condenser.

In Eq. (14), the refrigerant temperature at elemental volume inlet is considered during the single-phase flow whereas the average refrigerant saturation temperature at elemental volume inlet–outlet is used during the condensation regime. In the latter situation, Eq. (14) has to be solved together with Eq. (2) since refrigerant-side pressure drop affects saturation temperature which, in turn, influences heat transfer rate.

2.4. Circuits splitting and merging

Splitting or merging of single circuits are feasible ways that may be used in condenser design to reduce the refrigerant-side pressure drop, through circuit mass flow rate reduction, to enhance refrigerant-side heat transfer coefficient, through circuit mass flow rate increase, or to separate condensing and subcooling area [12].

In the present model, both bend split/merge (Fig. 4(a)) and the header split/merge (Fig. 4(b)) can be handled and the mass, momentum and energy equations that are introduced to describe them are different depending if a circuit splitting or a circuit merging is considered. Merging and splitting processes are supposed to be isobaric and the pressure drop caused by the merging or splitting component is neglected.

Therefore, the following equations apply for the description of a merging component (n is the number of circuits that merge into one):

$$\sum_{i=1}^{n} \dot{m}_{REF,IN,i} = \dot{m}_{REF,OUT} \tag{20}$$

$$p_{REF,IN,1} = p_{REF,IN,2} = \cdots = p_{REF,IN,n} = p_{REF,OUT} \tag{21}$$

$$\sum_{i=1}^{n} \dot{m}_{REF,IN,i} h_{REF,IN,i} = \dot{m}_{REF,OUT} h_{REF,OUT} \tag{22}$$

Under the hypotheses previously introduced, the momentum equation for a merging component becomes Eq. (21) where it is stated that the pressure of the refrigerant at merging component outlet is equal to the pressure of the refrigerant at the end of each merging circuit (inlet of merging component). This influences the pressure drop of each merging circuit since it has to be adapted so that the refrigerant pressure at the end of each merging circuit (inlet of merging component) is the same. In the present model this issue is handled iteratively, imposing the refrigerant mass flow rate in each merging circuit (an even distribution is used as initial guess value) and solving mass, momentum and energy equations for each of them. Once each merging circuit is solved, a check on the refrigerant pressure at their end is performed. If all the pressures are
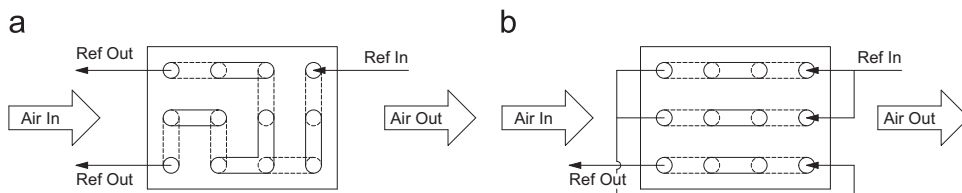

Fig. 4. Circuit bend splitting (a) and header merging (b) in condenser circuitry.

equal, the refrigerant mass flow rate distribution among each circuit is appropriate and each merging circuit is properly solved, otherwise each of the guessed refrigerant mass flow rate is modified introducing a correction coefficient calculated as the square root of the ratio between the considered circuit pressure drop and the average pressure drop of all merging circuits [3]. It is worth noting that the same procedure is used on a condenser scale to appropriately distribute refrigerant mass flow rate between the inlet and the outlet headers.

The splitting component is described through the following equations (m is the number of circuits that split from one circuit):

$$\dot{m}_{REF,IN} = \sum_{j=1}^{m} \dot{m}_{REF,OUT,j} \tag{23}$$

$$p_{REF,IN} = p_{REF,OUT,1} = p_{REF,OUT,2} = \cdots = p_{REF,OUT,m} \tag{24}$$

$$h_{REF,IN} = h_{REF,OUT,1} = h_{REF,OUT,2} = \cdots = h_{REF,OUT,m} \tag{25}$$

For a splitting component a similar issue arises for the refrigerant mass flow rate distribution among the different circuits that originates from it since, again, the refrigerant mass flow rate that feeds each split circuit is inversely proportional to the pressure drop of the split circuit. The same procedure used to calculate the refrigerant mass flow rate distribution at the inlet of a merging component is used to calculate refrigerant mass flow rate distribution at the outlet of a splitting component.

2.5. Transition element

At the elemental volume level, on the refrigerant-side, it is possible to have a single-phase inlet condition and a two-phase outlet condition (from superheated vapour to liquid–vapour mixture) or a two-phase inlet condition and a single-phase outlet one (from liquid–vapour mixture to subcooled liquid). The elemental volume where transition from single-phase to two-phase or vice versa happens is usually referred to as transition element. In the present model, it is assumed that the refrigerant properties are constant at the elemental volume level and, moreover, the appropriate correlations for the calculation of pressure drop and heat transfer coefficient are automatically chosen according to the refrigerant state at elemental volume inlet. This may lead to an improper handling of transition element which, in turn, may introduce significant errors in heat transfer rate and in subcooling calculation [15]. In order to address this issue, different tracking techniques to locate the phase change boundary are proposed and compared [14] in order to find the best compromise between accuracy and computational time. In the present paper the technique proposed by Iu et al. [15] is used to account for transition element.

3. Model validation

The model is validated using experimental data of two small fin-and-tube condenser whose geometry is identical except for the overall number of fins (in the following the condenser with the lowest number of fins is referred to as Condenser A whereas the condenser with the highest number of fins is referred to as Condenser B). The geometry of both condensers is provided in Table 1 whereas the circuit arrangement is shown in Fig. 5.

Prior to the model validation, a sensitivity analysis of the condenser heat transfer rate and refrigerant-side pressure drop on the number of elemental volumes per tube is done. The analysis is carried out only for Condenser B and considering a refrigerant mass flow rate equal to $\dot{m}_{REF} = 43.4$ kg h^{-1} and an air frontal velocity equal to $v_{AIR} = 2.9$ m s^{-1}, which is the working condition where the condenser heat transfer rate is the maximum one. The number of elemental volumes used to divide the tube is discretely increased from 1 (meaning that the only elemental volume includes all the fins) to 70 (meaning that each elemental volume includes one single fin) and the results of condenser heat transfer rate and the refrigerant-side pressure drop are reported in Fig. 6. It is possible to note that the condenser heat transfer rate increases remarkably first and

Table 1
Condenser geometrical parameters.

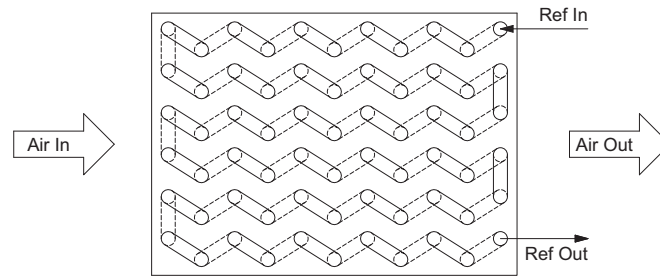| Tube		Fins	
Material	Aluminium	Material	Aluminium
Type	Smooth	Type	Plain
Internal diameter (mm)	6.6	Thickness (mm)	0.15
External diameter (mm)	8	Pitch$_A$ (mm)	3.24
Length (mm)	178	Pitch$_B$ (mm)	2.54
Transversal pitch (mm)	25.33		
Longitudinal pitch (mm)	19		

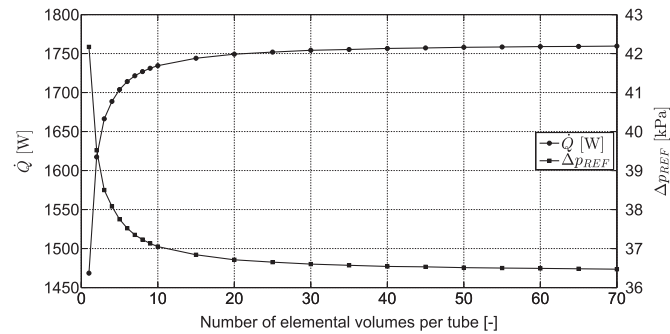**Fig. 5.** Circuitry of the condenser used for model validation.

Fig. 6. Sensitivity analysis of the number of the condenser heat transfer rate and refrigerant-side performance to the number of elemental volumes per tube.

then levels off as the number of elemental volumes per tube increases, whereas the opposite happens for refrigerant-side pressure drop, and that both parameters are within $\pm 1\%$ of the asymptotic value when the number of elemental volumes per tube is greater than 15. As a result, a number of elemental volumes per tube equal to 20 is chosen to simulate the Condenser B as a good compromise between simulation accuracy and computation speed. The same analysis is carried out for Condenser A finding that 11 elemental volumes per tube are enough to accurately simulate the fin-and-tube condenser.

Three different working conditions for each condenser are available from manufacturer data for fin-and-tube condenser validation. Test conditions are shown in Table 2 (first line of refrigerant mass flow rate refers to Condenser A whereas the second line to Condenser B) while tests are carried out in a test rig that imposes uniform distribution both for air velocity and temperature. Each test is repeated twice and for each test condenser heat transfer rate and refrigerant-side pressure drop are measured and their value is compared to the one calculated by the model where the refrigerant properties are calculated using Refprop 9.1 [18]. The results of the comparison are provided in Fig. 7(a) and (b) respectively where a very good agreement between the experimental and numerical results is shown since the difference among them spans the range -3.06% to $+4.09\%$ for the condenser heat transfer rate, resulting in a good capability of heat transfer rate prediction, and in the range -1.40% to +20.98% for the refrigerant-side pressure drop, resulting in a slight tendency in over-predicting refrigerant-side pressure drop. Overall, the developed model is considered as a reliable tool to be used to predict condenser performance varying heat exchanger geometry or working conditions.

4. Circuitry analysis

Once the model is validated against experimental data, it is used to analyse the influence of circuit arrangement on condenser performance. Indeed, as shown in Fig. 5, both condensers are provided with only one refrigerant circuit that

Table 2
Experimental test conditions.

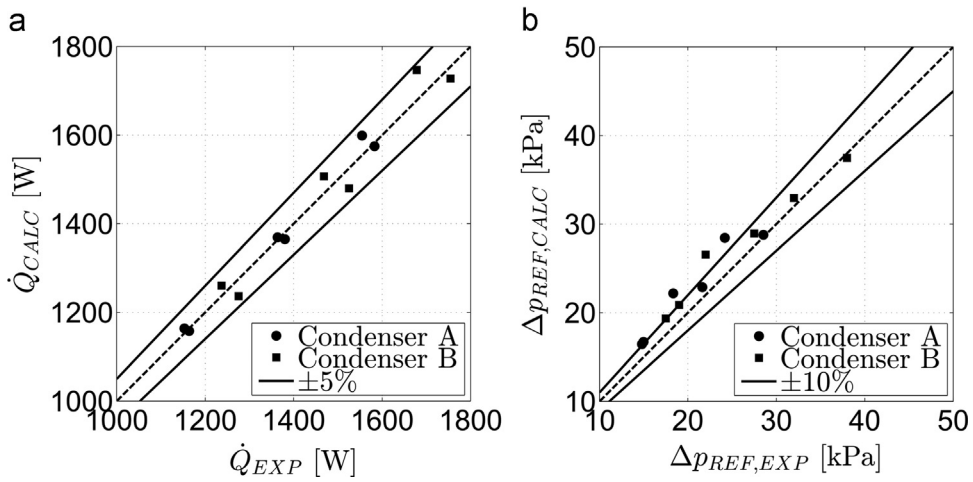| Variable	Value
Refrigerant mass flow rate [kg·h^{-1}]	28.8, 34.2, 39.3
	31.6, 37.8, 43.4
Refrigerant inlet pressure (kPa)	2116
Refrigerant inlet temperature (K)	355.15
Air frontal velocity (m s^{-1})	1.9, 2.4, 2.9
Air inlet temperature (K)	318.15

Fig. 7. Parity plot of the condensers capacity (a) and of the refrigerant-side pressure drop (b).
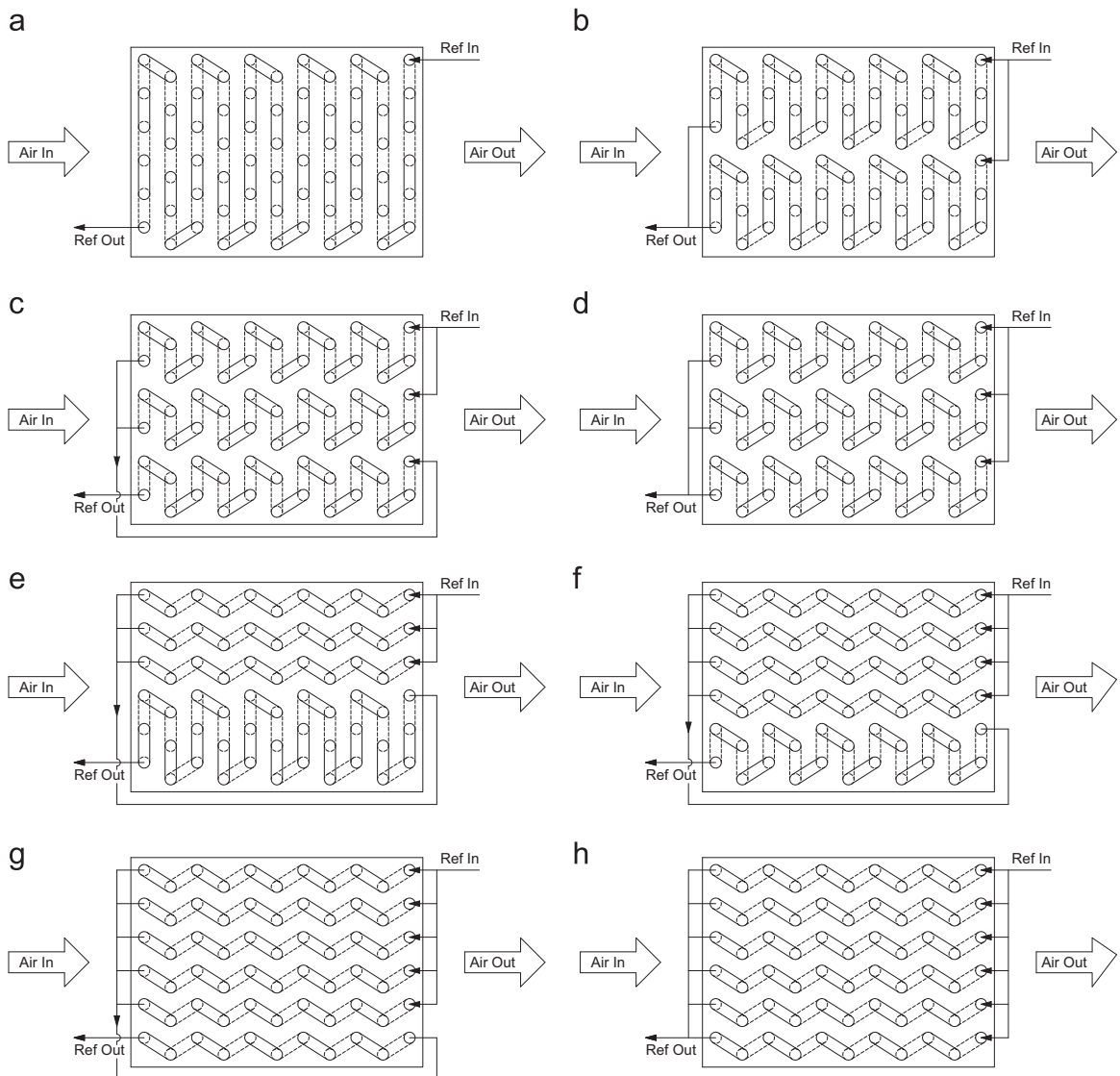

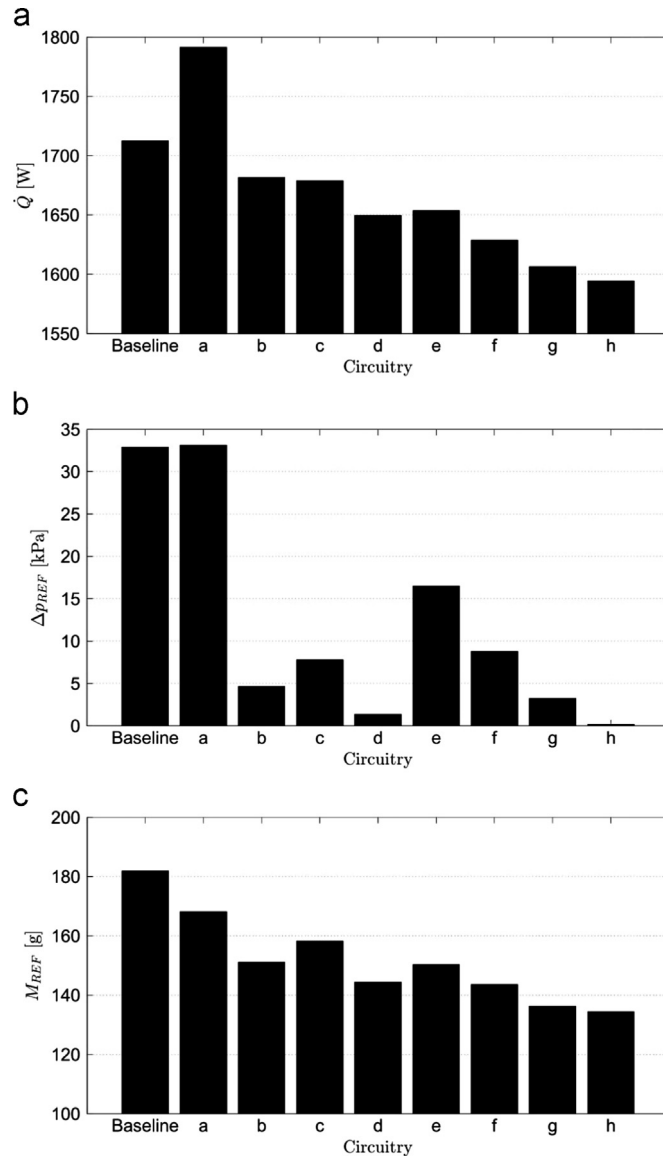**Fig. 8.** Condenser circuitries analysed.

Fig. 9. Heat transfer rate (a), refrigerant-side pressure drop (b) and refrigerant charge variation (c) with respect to the baseline for each of the circuit arrangements considered.

makes the mean refrigerant direction either counter-flow or parallel-flow with respect to the air flow one. However, it is well known that the best flow arrangement in a heat exchanger is the counter-flow one [26] and, furthermore, one single circuit results in higher refrigerant heat transfer coefficient, that leads to higher condenser heat transfer rate, but also in high refrigerant-side pressure drop, that leads to high compressor work. Therefore, different circuit arrangements are investigated with the aim of either increasing the condenser heat transfer rate or reducing refrigerant-side pressure drop considering several circuit arrangements leading to a mean counter-flow arrangement as shown in Fig. 8. It is worth specifying that, for the sake of simplicity, simulations are carried out only for Condenser B, that is the condenser with the lower fin pitch, and considering a refrigerant mass flow rate equal to $\dot{m}_{REF} = 43.4 \text{ kg h}^{-1}$ and an air frontal velocity equal to $v_{AIR} = 2.9 \text{ m s}^{-1}$, which is the working condition where the condenser heat transfer rate is the maximum one.

The variation of condenser heat transfer rate, refrigerant-side pressure drop and refrigerant charge as a function of circuit arrangement are shown in Fig. 9(a), (b) and (c) respectively where the values of the baseline arrangement are shown for the sake of comparison. The results show that the condenser heat transfer rate increases when the circuit arrangement allows for a mean counter-flow direction between refrigerant and air (+4.61% arrangement (a) versus baseline) whereas it reduces as the number of circuits increases (arrangements (b)–(h)), although the mean counter-flow arrangement is obtained, since the increase of the circuits' number leads to the reduction of the refrigerant mass flow rate flowing in each of them and, consequently, to the reduction of the convective heat transfer coefficient which, in turn, negatively influences the overall

condenser heat transfer rate. The use of circuits merging may slightly increase the heat transfer rate provided that the heat transfer area allocated to the merged circuit is greater than the heat transfer area allocated to each single merging circuit (compare arrangement (b)–(c) and (d)–(e)).

The refrigerant-side pressure drop is nearly constant (+1.06%, arrangement (a) versus baseline) or strongly reduces when the number of circuit increases due to refrigerant mass flow rate reduction, even when circuits' merging is considered. In the last situation, an increase of refrigerant-side pressure drop is observed due to the increase of refrigerant mass flow rate after merging (compare arrangement (b)–(c) and (d)–(e)).

Finally, a general reduction trend of the refrigerant charge trapped inside the condenser with the increase of the number of circuit is found. This is particularly evident if baseline arrangement is compared to arrangements (b), (d) and (h) respectively and, with the only exception of arrangement (a), it may be interpreted keeping in mind that the condenser heat transfer rate reduces as the number of circuits increases. This leads, at the outlet of the condenser, to the reduction of the refrigerant subcooling or, even more, to a two-phase flow (e.g. this happens for arrangements (d) and (h)) making the condenser mean void fraction progressively to increase since its internal volume becomes "less filled" with refrigerant in the liquid state and "more filled" with refrigerant in the vapour state. Since the vapour density is lower than the liquid one, the overall refrigerant charge reduces. The analysis of refrigerant charge for arrangement (a) is more tricky since an increase of condenser heat transfer rate equal to +4.61% but a reduction of refrigerant charge equal to −7.56% are found. This trend is not trivial since the increase of condenser heat transfer rate found for arrangement (a) arises from an increase of refrigerant subcooling and condenser outlet. Since the refrigerant is in liquid state, the refrigerant charge is expected to be higher. However, a closer inspection of condenser working conditions reveals that vapour desuperheating requires, in the baseline arrangement, the first nine tubes whereas in the arrangement (a) 12 tubes (the last two rows) are needed due to lower refrigerant-to-air temperature difference. Moreover, although the overall area needed for full condensation is lower for arrangement (a) than for baseline arrangement (52 tubes versus 57), the average void fraction in the two-phase area is greater in the former arrangement since, again, the refrigerant-to-air temperature difference is strongly reduced at the beginning of the condensation process. Indeed, due to counter-flow arrangement, for a quality variation from 1 to 0.6 (void fraction from 1 to 0.9) 30 tubes are needed in arrangement (a) and 25 tubes in baseline arrangement, making in the former situation the great part of the condensation area filled with a high void fraction two-phase mixture. As a result, compared to baseline, the arrangement (a) is filled with refrigerant whose density is generally closer to the vapour one (36 tubes versus 31) making the mass trapped in the condenser lower. As a result, the condenser heat transfer rate per unit of refrigerant mass passes from 9.41 W g^{-1} in the baseline arrangement to 10.65 W g^{-1} in (a) arrangement, resulting in a substantial improvement in condenser performance.

5. Conclusions

In the present paper a model for the simulation of fin-and-tube condenser has been developed. The model is based on a finite volume approach that divides each tube in small elemental volumes where mass, momentum and energy equations are solved using the effectiveness-NTU method and with the help of the most updated correlations for void fraction, pressure drop and heat transfer coefficient calculation. The model is able to account for any working conditions, for complex refrigerant circuitry and bi-dimensional air mal-distribution, making possible to use it either in a design process or in a performance analysis process. The model is validated against experimental data on a small capacity condenser finding a good agreement with respect to condenser capacity, refrigerant-side pressure drop and air-side pressure drop. The model is then used to analyse the influence of some simple circuit arrangements on the condenser performance. With the help of the model it is demonstrated that the configuration of the circuit is very important in designing fin-and-tube condenser since enhancement of condenser heat transfer rate with the same refrigerant-side pressure drop and reduced refrigerant charge may be achieved simply by modifying the refrigerant path.

References

[1] H.M.M. Afroz, A. Miyara, Friction factor correlation and pressure loss of single phase flow inside herringbone microfin tubes, Int. J. Refrig. 30 (2007) 1187–1194.
[2] A. Bensafi, S. Borg, D. Parent, CYRANO: a computational model for the detailed design of plate-fin-and-tube heat exchangers using pure and mixed refrigerants, Int. J. Refrig. 20 (1997) 218–228.
[3] V. Casson, A. Cavallini, L. Cecchinato, D. Del Col, L. Doretti, E. Fornasieri, L. Rossetto, C. Zilio, Performance of finned coil condensers optimized for new HFC refrigerants, ASHRAE Trans. 108 (2) (2002) 517–528.
[4] A. Cavallini, D. Del Col, L. Doretti, G.A. Longo, L. Rossetto, Heat transfer and pressure drop during condensation of refrigerants inside horizontal enhanced tubes, Int. J. Refrig. 23 (2000) 4–25.
[5] A. Cavallini, D. del Col, S. Mancin, L. Rossetto, Condensation of pure and near-azeotropic refrigerants in microfin tubes: a new computational procedure, Int. J. Refrig. 32 (2009) 162–174.
[6] J.B. Copetti, M.H. Macagnan, D. de Souza, R. de Césaro Oliveski, Experiments with micro-fin tube in single phase, Int. J. Refrig. 27 (2004) 876–883.
[7] W.K. Ding, J.F. Fan, Y.L. He, W.Q. Tao, Y.X. Zheng, Y.F. Gao, J. Song, A general simulation model for performance prediction of plate fin-and-tube heat exchanger with complex circuit configuration, Appl. Thermal Eng. 31 (2011) 3106–3116.
[8] P.A. Domanski, EVAP-COND simulation models for finned tube heat exchangers, National Institute of Standards and Technology Building and Fire Research Laboratory, Gaithersburg, MD, USA, 2003.

[9] P.A. Domanski, D. Yashar, Optimization of finned-tube condensers using an intelligent system, Int. J. Refrig. 30 (2007) 482–488.
[10] J. el Hajal, J.R. Thome, A. Cavallini, Condensation in horizontal tubes, Part 1: two-phase flow pattern map, Int. J. Heat Mass Transf. 46 (2003) 3349–3363.
[11] ESDU, 2014. Design and performance evaluation of heat exchangers: the effectiveness-NTU method: Part 3: graphical and analytical data. ESDU International PLC.
[12] E. Fornasieri, C. Zilio, An aspect of condenser optimization in refrigeration plants (in Italian), in: Proceedings of 39th AiCARR International Conference, 1998, pp. 605–616.
[13] V. Gnielinski, On heat transfer in tubes, Int. J. Heat Mass Transf. 63 (2013) 134–140.
[14] L. Huang, V. Aute, R. Radermacher, A finite volume coaxial heat exchanger model with moving boundaries and modifications to correlations for two-phase flow in fluted annuli, Int. J. Refrig. 40 (2014) 11–23.
[15] I. Iu, N.A. Weber, P. Bansal, D.E. Fisher, Applying the effectiveness-NTU method to elemental heat exchanger model, ASHRAE Trans. 113 (1) (2007) 504–513.
[16] H. Jiang, V. Aute, R. Radermacher, Coil designer: a general-purpose simulation and design tool for air-to-refrigerant heat exchangers, Int. J. Refrig. 29 (2006) 601–610.
[17] W.M. Kays, A.L. London, Compact Heat Exchangers, McGraw Hill, New York, 1984.
[18] E.W. Lemmon, M.L. Huber, M.O. McLinden. NIST standard reference database 23: reference fluid thermodynamic and transport properties-REFPROP, version 9.1. National Institute of Standards and Technology, Standard Reference Data Program, Gaithersburg, MD, USA, 2013.
[19] J. Liu, W.J. Wei, G.L. Ding, C. Zhang, M. Fukaya, K. Wang, T. Inagaki, A general steady state mathematical model for fin-and-tube heat exchanger based on graph theory, Int. J. Refrig. 27 (2004) 965–973.
[20] J.M. Quibén, J.R. Thome, Flow pattern based two-phase frictional pressure drop model for horizontal tubes, Part II: new phenomenological model, Int. J. Heat Fluid Flow 28 (2007) 1060–1072.
[21] H. Schlichting, K. Gersten, Boundary Layer Theory, Springer, Berlin, 2000.
[22] V. Singh, V. Aute, R. Radermacher, Numerical approach for modeling air-to-refrigerant fin-and-tube heat exchanger with tube-to-tube heat transfer, Int. J. Refrig. 31 (2008) 1414–1425.
[23] J.R. Thome, J. el Hajal, A. Cavallini, Condensation in horizontal tubes, Part 2: new heat transfer model based on flow regimes, Int. J. Heat Mass Transf. 46 (2003) 3365–3387.
[24] C.-C. Wang, K.-Y. Chi, C.-J. Chang, Heat transfer and friction characteristics of plain fin-and-tube heat exchangers, Part II: Correlation, Int. J. Heat Mass Transf. 43 (2000) 2693–2700.
[25] C.C. Wang, W.L. Fu, C.T. Chang, Heat transfer and friction characteristic of typical wavy fin-and-tube heat exchangers, Exp. Therm. Fluid Sci. 14 (1997) 174–186.
[26] C.-C. Wang, J.-Y. Jang, C.-C. Lai, Y.-J. Chang, Effect of circuit arrangement on the performance of air-cooled condensers, Int. J. Refrig. 22 (1999) 275–282.
[27] C.-C. Wang, C.-J. Lee, C.-T. Chang, S.-P. Lin, Heat transfer and friction correlation for compact louvered fin-and-tube heat exchangers, Int. J. Heat Mass Transf. 42 (1999) 1945–1956.
[28] Z. Wu, G. Ding, K. Wang, M. Fukaya, Application of a genetic algorithm to optimize the refrigerant circuit of fin-and-tube heat exchangers for maximum heat transfer or shortest tube, Int. J. Therm. Sci. 47 (2008) 985–997.
[29] H.-Y. Ye, K.-S. Lee, Refrigerant circuitry design of fin-and-tube condenser based on entropy generation minimization, Int. J. Refrig. 35 (2012) 1430–1438.